Fusion cross sections for the ^{9}Be+^{124}Sn reaction at energies near the Coulomb barrier

V. V. Parkar,[1,*,†] R. Palit,[1] Sushil K. Sharma,[1] B. S. Naidu,[1] S. Santra,[2] P. K. Joshi,[3] P. K. Rath,[4] K. Mahata,[2] K. Ramachandran,[2] T. Trivedi,[5] and A. Raghav[6]

[1]*Department of Nuclear and Atomic Physics, Tata Institute of Fundamental Research, Mumbai 400005, India*

[2]*Nuclear Physics Division, Bhabha Atomic Research Centre, Mumbai 400085, India*

[3]*Homi Bhabha Centre for Science Education, Tata Institute of Fundamental Research, Mumbai 400088, India*

[4]*Department of Physics, M.S. University of Baroda, Vadodara 390002, India*

[5]*Department of Physics, University of Allahabad, Allahabad 211001, India*

[6]*Department of Physics, University of Mumbai, Mumbai 400098, India*

(Received 19 April 2010; revised manuscript received 9 July 2010; published 3 November 2010)

The complete and incomplete fusion cross sections for ^{9}Be+^{124}Sn reaction have been deduced using the online γ-ray measurement technique. Complete fusion at energies above the Coulomb barrier was found to be suppressed by ∼28% compared to the coupled-channels calculations and is in agreement with the systematics of L. R. Gasques *et al.* [Phys. Rev. C **79**, 034605 (2009)]. Study of the projectile dependence for fusion on a ^{124}Sn target shows that, for ^{9}Be nuclei, the enhancement at below-barrier energies is substantial compared to that of tightly bound nuclei.

DOI: 10.1103/PhysRevC.82.054601 PACS number(s): 25.70.Jj, 25.60.Pj, 25.70.Mn

I. INTRODUCTION

^{6,7}Li, ^{9}Be, and ^{10,11}B nuclei, having an $\alpha + x$ cluster structure and low threshold energies for breakup into two or more fragments, are nowadays increasingly used as projectiles to study nuclear structure and reaction dynamics [1,2]. In the study of nuclear structure, incomplete fusion (ICF) (the process in which part of the projectile is captured by the target) is used as an effective tool in populations of relatively neutron-rich nuclei as well as the narrow spin distribution in compound systems compared to complete fusion (CF) (the process in which the whole projectile fuses with the target). In the case of study of reaction dynamics, fusion involving such loosely bound stable/unstable projectiles is of interest for astrophysics and for superheavy element formation. The recent availability of light-mass radioactive ion beams such as ^{6,8}He, ^{11}Be, and ^{17}F has also generated a renewed interest in the preceding topic. For unstable nuclei, the fusion process is affected by their low binding energy, which can cause them to break up before reaching the fusion barrier. Thus the breakup process may reduce the CF cross sections, making it difficult in superheavy element formation. Alternatively, the extended structure of loosely bound nuclei could in principle induce a large enhancement of fusion. Observations of these effects on fusion have proven to be controversial [3–6].

It has been observed that CF is suppressed by ∼32% for ^{9}Be+^{208}Pb and ^{209}Bi [6,7] and ∼10% for ^{9}Be+^{144}Sm [8], and this observation has been attributed to the breakup of ^{9}Be, leading to loss of flux from the CF channel. In contrast, the study of fusion of ^{9}Be with light-mass targets, namely, ^{27}Al [9] and ^{64}Zn [10], has drawn a different conclusion. The authors do not report any suppression and, also, conclude that for these systems nuclear breakup is the dominant process that occurs at short distances, and thus it does not inhibit the fusion process. However, contrary to the aforementioned conclusions, exclusive breakup measurements carried out for the ^{9}Be+^{208}Pb system [11] report the breakup of ^{9}Be to be associated with nuclear surface interactions.

Recently, Gasques *et al.* [12] reviewed the data available for fusion cross sections of ^{6,7}Li, ^{9}Be, and ^{10,11}B projectiles and showed the systematics of the fusion suppression factor, F_{CF} (ratio of the measured CF cross sections to those expected from calculations without breakup coupling), as a function of the charge product of the projectile and the target $Z_P Z_T$. They observed that CF suppression for reactions involving ^{6,7}Li and ^{10}B projectiles are rather independent of the target mass. It was also observed that suppression is the largest for reactions involving a ^{6}Li projectile, which has the lowest breakup threshold. However, for ^{9}Be-induced fusion reactions, the values of F_{CF} did not follow a systematic trend. Especially, the fusion suppression factor for the ^{9}Be+^{144}Sm reaction was reported to be much lower compared to that for systems involving heavier targets. To understand this behavior and investigate further the effect of breakup for ^{9}Be-induced reactions, we have measured fusion cross sections involving the nearby medium-mass target ^{124}Sn. As the target nucleus is proton shell closed and spherical, the effect of target inelastic excitation on fusion will be less important compared to the effect caused by projectile breakup. This allowed us to single out the effect of breakup more prominently.

Because all evaporation residues (ERs) populated in the ^{9}Be+^{124}Sn reaction are stable nuclei, we adopted the technique of online γ-ray measurements. Details of the experimental setup for ER measurements are reported in Sec. II. The results for ER and fusion cross sections, coupled-channels (CC) calculations, and discussion are presented in Sec. III. A summary and conclusions of the present study are given in Sec. IV.

II. EXPERIMENTAL DETAILS

The experiment was performed using a ^{9}Be beam at energies $E_{\mathrm{beam}} = 26$–38 MeV, in steps of 1 MeV, at the 14UD

*parkarvivek@gmail.com

†Present address: Departamento de Física Aplicada, Universidad de Huelva, E-21071 Huelva, Spain.

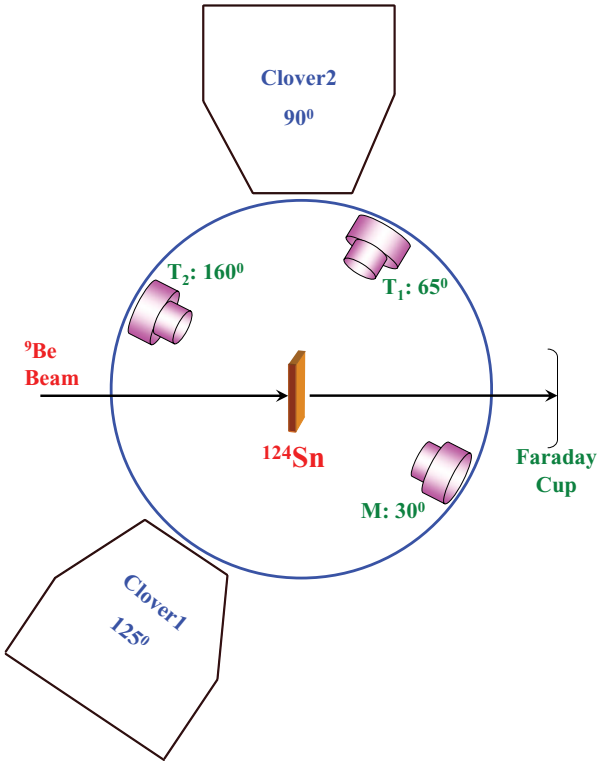

FIG. 1. (Color online) Schematic illustration of experimental setup used for measurement of the fusion cross section in the ^{9}Be+^{124}Sn reaction.

BARC-TIFR Pelletron accelerator, Mumbai. The target used was ^{124}Sn of thickness 2.47 ± 0.04 mg/cm^2, which was measured using the Rutherford backscattering method. Energies were corrected for the loss at half the target thickness and used in the further analysis. A new compact scattering chamber, 24 cm in diameter, which can contain the charged particle detectors and target assembly, was designed, fabricated, and used for this experiment. The chamber was made of aluminum alloy, to reduce attenuation of the γ energies. Before its entry into the scattering chamber, the beam was defined by two square collimators of 3 × 3 and 2 × 2 mm^2, respectively, separated by a distance of 1 m. The target was located 1.9 m downstream from the last collimator. A schematic illustration of the experimental setup is shown in Fig. 1. Two Compton suppressed clover detectors were placed outside the scattering chamber in the horizontal plane at a distance of 25 cm from the target center: one at 125°, for absolute cross-section estimation of various reaction channels, and the other at 90°, for identification of unshifted γ lines. The absolute efficiency of both detectors was determined using a set of calibrated radioactive sources (^{152}Eu, ^{133}Ba, and ^{60}Co) mounted with the same geometry as the target. Along with the clover detectors, two charged-particle detector telescopes (ΔE = 20–30 μm, E = 1000 μm) and one monitor detector (=500 μm) were placed at 65°, 160°, and 30°, respectively. The monitor detector angle was chosen in such a way that even at the highest bombarding energy, elastic scattering remains in the Rutherford scattering regime. The solid angles of the telescopes and monitor detector were deduced accurately by measuring elastic (Rutherford) scattering from a ^{209}Bi target of known thickness (∼300 μg/cm^2) at $E_{\rm beam}$ = 26 MeV. The integrated beam current deposited at the beam dump after the target was also recorded using a high-precision current integrator, calibrated using a Keithley current source. Data were acquired and stored in an event-by-event list mode, in the particle-γ OR condition. The coincidence between the 125° clover detector and the particle telescopes (TAC1, TAC2) was also recorded in the ADC. We used the FERA-based data acquisition system developed for the INGA (Indian National Gamma Array) campaign at the BARC-TIFR accelerator facility, for handling these high count rates in the OR condition. These TAC spectra were further utilized for putting the gates in the γ-ray spectra and identifying γ lines of ERs from the ICF process.

III. RESULTS AND DISCUSSION

A. Data reduction

The compound nucleus following the CF of ^{9}Be+^{124}Sn formed in this reaction is ^{133}Xe, which decays predominantly by neutron emission, producing ERs. The γ rays from these ERs have been identified in the current experimental setup. The typical γ-ray add-back spectrum from the clover detector at 125° and $E_{\rm beam}$ = 38 MeV is shown in Fig. 2. The γ lines from ERs following CF and ICF processes are identified and labeled. In Fig. 2, the labels α, 1n and α, 2n correspond to the ERs when part of the projectile (α) fuses with the target and then evaporates 1n and 2n, respectively. ICF of ^{8}Be with ^{124}Sn will produce the same ERs as does CF of ^{9}Be with ^{124}Sn. Hence it is not possible to separate the contribution from these two processes in the present setup. Breakup neutron and γ-ray coincidence measurements are required to measure this channel.

Emission cross sections for γ transitions of interest were calculated from the relation

$$\sigma_\gamma(J) = \frac{Y_\gamma(J)}{Y_M}\frac{d\Omega_M}{E_\gamma}\sigma_M,$$

where $Y_\gamma(J)$ is the yield of that γ line after correcting for the internal conversion, Y_M is the monitor yield, $d\Omega_M$ is

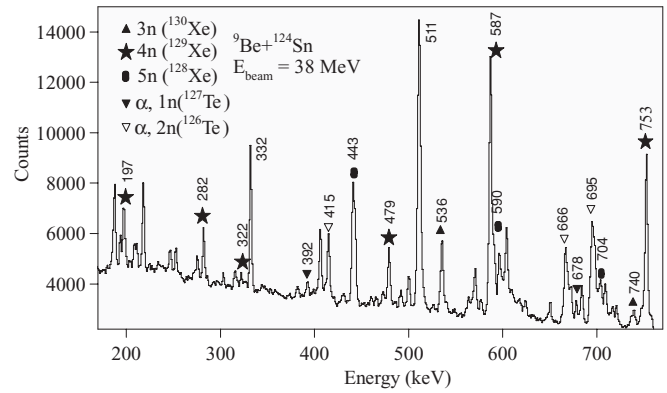

FIG. 2. γ-ray add-back spectrum from the clover detector at 125° and $E_{\rm beam}$ = 38 MeV. The γ lines from the possible evaporation residues following CF are labeled. The γ lines following the ICF channel are also labeled as (α, 1n) and (α, 2n).

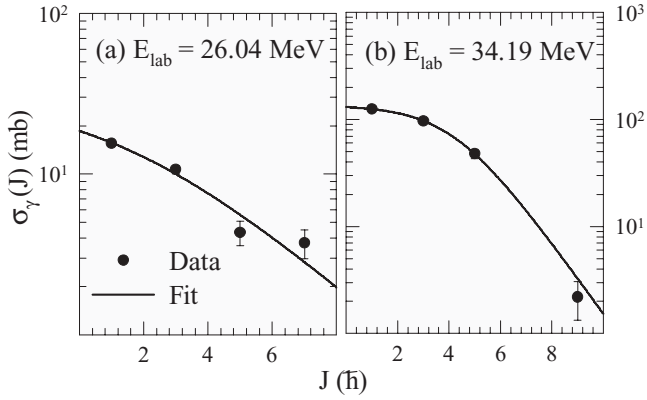

FIG. 3. Typical extrapolation method for obtaining the cross sections at $J = 0$ are shown for two energies, (a) a lower energy, $E_{lab} = 26.04$ MeV, and (b) a higher energy, $E_{lab} = 34.19$ MeV, both for ^{130}Xe residues. The equation $\sigma_\gamma(J) = a/\{1 + \exp[-(J - J_0)/b]\}$ was used for fitting and to get the value at $J = 0$.

the solid angle of the monitor detector, E_γ is the absolute efficiency of the γ lines, and σ_M is the Rutherford cross section (at $\theta_M = 30^\circ$) at the same beam energy. For even-even ERs (^{130}Xe, ^{128}Xe, and ^{126}Te) the γ-ray cross sections $\sigma_\gamma(J)$, for various transitions in the ground-state rotational band [13–15] are plotted as a function of J and then further extrapolated up to $J = 0$, to get the corresponding ER cross sections as in Refs. [3] and [5]. In particular, the cross sections for the population of the first four excited states of the yrast band of ^{130}Xe, obtained from the yields of 536.2, 668.6, 739.6, and 752.8 keV transitions are shown in Fig. 3, along with the fit. The equation $\sigma_\gamma(J) = a/\{1 + \exp[-(J - J_0)/b]\}$ is used for fitting of the experimental J distribution and extrapolation to $J = 0$. In this expression a, b, and J_0 correspond to the normalization constant, the diffuseness of the J distribution, and the value of J at which $\sigma_\gamma(J)$ becomes half of its maximum, respectively. For the odd-mass ^{129}Xe [16] ($4n$ channel), cross sections were obtained using the measured intensities of the $\frac{11}{2}^-$ state at 587 keV and normalizing them with the results of the $4n$ channel from the statistical model code PACE [17]. Note that the cross sections for the experimental $3n$ and $5n$ (even-mass) channels showed a good agreement with those from PACE predictions. These experimental ER cross sections are shown in Fig. 4. Cross sections for $3n$, $4n$, and $5n$ ERs from CF are represented by filled circles, open circles, and filled stars, respectively. Open triangles correspond to cross sections for the formation of ^{126}Te (ICF; α, $2n$). Determination of the cross section for the formation of ^{127}Te (ICF; α, $1n$) was not possible, owing to its little-known level structure [15].

In the PACE calculations, the cross section for each partial wave (ℓ distribution), obtained from the CC calculation code CCFULL [18] in the uncoupled mode, were fed as input. The default optical potentials available in PACE were retained. The only free parameter remaining in the PACE input was the level density parameter a, which showed a negligible dependence on the values between $a = A/9$ and $a = A/10$. According to these PACE predictions, the sum of $3n$, $4n$, and $5n$ ERs contributes about 94–98% of the total CF. The missing ER contributions to the total CF have been corrected using these

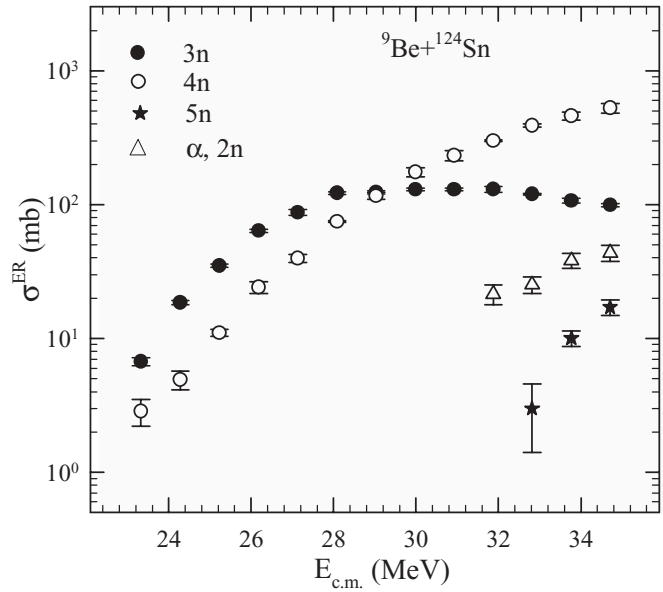

FIG. 4. Experimental ER cross sections for $3n$, $4n$, and $5n$ evaporation from CF are represented by filled circles, open circles, and filled stars, respectively. Open triangles correspond to cross sections for $2n$ evaporation from the ICF generated by the capture of α by the target.

PACE calculations as per the procedure mentioned in Ref. [19]; that is, $\sigma_{fus}^{exp} = \sum_x \sigma_{xn}^{exp}/R$. Here, the ratio R is defined as $R = \sum_x \sigma_{xn}^{PACE}/\sigma_{fus}^{PACE}$, where $x = 3, 4, 5$, etc. These values of the ratio R and the CF cross sections thus obtained are listed in Table I.

These CF cross sections are shown by filled circles in Fig. 5(a). From these CF cross sections, the fusion barrier distribution was derived using the expression $d^2\sigma_{fus}^{exp} E_{c.m.}/dE_{c.m.}^2$ and is represented by filled circles in Fig. 5(b). The average experimental barrier position was obtained by fitting this barrier distribution with a Gaussian, the peak of which was found to be 25.87 ± 0.07 MeV.

TABLE I. Experimental fusion cross sections along with the ratio R (defined in the text) for the ^{9}Be+^{124}Sn reaction in the measured energy range.

E_{lab} (MeV)	$E_{c.m.}$ (MeV)	R	σ_{fus} (mb)
25.02	23.33	0.9455	10.1 ± 0.8
26.04	24.28	0.9659	24.3 ± 1.1
27.06	25.23	0.9739	47.3 ± 1.2
28.08	26.18	0.9800	89.6 ± 3.0
29.10	27.13	0.9830	129.3 ± 5.3
30.12	28.08	0.9844	200 ± 3
31.14	29.03	0.9851	244 ± 7
32.16	29.98	0.9851	322 ± 15
33.17	30.93	0.9834	369 ± 21
34.19	31.88	0.9841	437 ± 23
35.20	32.82	0.9832	517 ± 11
36.22	33.77	0.9818	584 ± 34
37.23	34.71	0.9806	656 ± 43

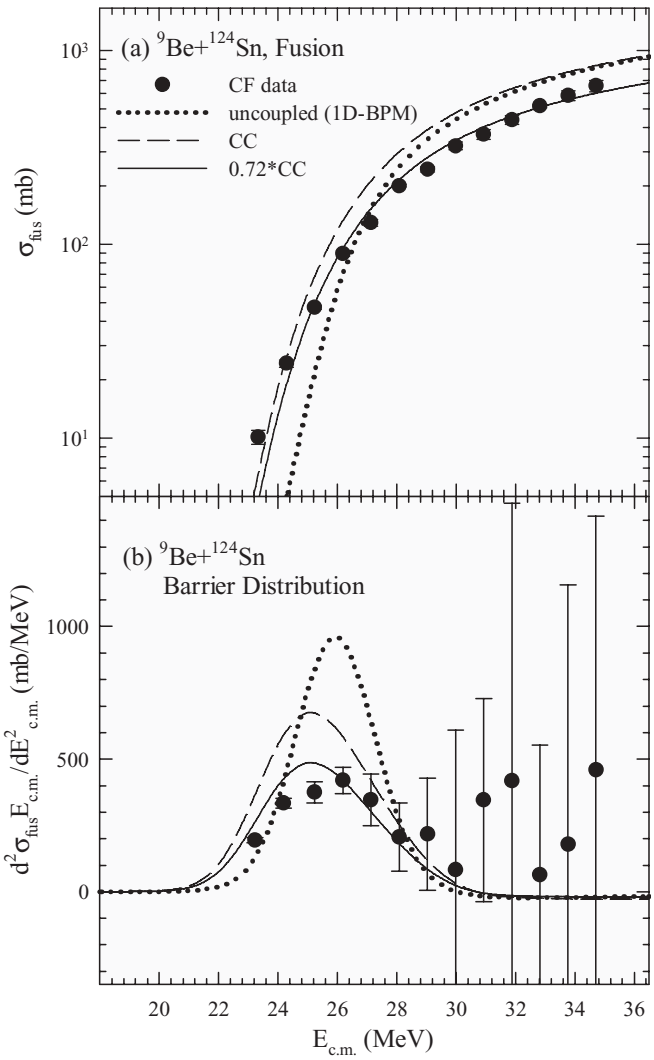

FIG. 5. (a) Complete fusion (CF) cross section (filled circles) and (b) corresponding barrier distribution (filled circles) for the ^{9}Be+^{124}Sn reaction compared with coupled (dashed lines) and uncoupled (dotted lines) results from CCFULL calculations. Solid lines were obtained by multiplying the coupled results by a suppression factor $F_{CF} = 0.72$.

B. Coupled-channels calculations

Simplified CC calculations were performed using the modified version of CCFULL [20], which allows coupling of the projectile excited states and includes the effect of the projectile ground-state spin. The initial input potential parameters for CCFULL were obtained from the Woods-Saxon parametrization of the Akyuz-Winther (AW) potential [21] (see Table II). Couplings to the ^{9}Be ground-state spin of $\frac{3}{2}^-$ with deformation parameter $\beta = 1.3$ [22], and the $\frac{5}{2}^-$ excited state in its $K = \frac{3}{2}^-$ ground-state rotational band with $E_x = 2.429$ MeV and $\beta = 0.72$ [23], were included. Target coupling included the 3^- vibrational excited state in ^{124}Sn with $E_x = 2.614$ MeV, $\beta = 0.153$ [24]. CCFULL calculations with shallow AW potentials led to oscillations of transmission coefficients of higher partial waves, especially at higher beam energies. To minimize such oscillations, the potential well was chosen to be deeper so that the ingoing wave boundary condition was correctly applied and such oscillations were minimized. Accordingly, the radius (r_0) and diffuseness (a_0) parameters of the potential were adjusted to reproduce the experimental barrier of 25.87 MeV. This modified potential for CC calculations is reported in Table II. The uncoupled (1D-BPM) and CC calculations are shown as dotted and dashed lines, respectively, in Fig. 5. It is interesting that when the calculated fusion cross sections obtained with the preceding full coupling are normalized by a factor $F_{CF} = 0.72$, the reduced fusion values (denoted by the solid line) reproduce the experimental fusion cross sections very well, especially at energies above the Coulomb barrier. This signifies that the measured CF cross sections are suppressed by 28%. The uncertainty in this number was estimated to be 5%, owing to the overall error in the measured fusion cross sections. Thus from Fig. 5(a) it can be concluded that the CC calculations overestimate the fusion cross section at above-barrier energies. At sub-barrier energies, the behavior appears to be different. Although there are only two data points at energies below the barrier, there seems to be a trend of enhancement in experimental fusion cross sections compared to calculations. Because the CC results at sub-barrier energies are highly influenced by coupling, which may be model dependent, as pointed out by Rath *et al.* [19], a strong conclusion regarding enhancement or suppression in this region is not possible.

TABLE II. Parameters for Akyuz-Winther (AW) and coupled-channels (CC) potentials, along with V_B, R_B, and $\hbar\omega$.

System	Potential	V_0 (MeV)	r_0 (fm)	a_0 (fm)	V_B (MeV)	R_B (fm)	$\hbar\omega$ (MeV)
^{9}Be+^{124}Sn	AW	49.251	1.175	0.628	26.01	10.38	4.13
	CC	130.250	0.992	0.800	25.87	10.25	3.71
^{40}Ca+^{124}Sn	AW	77.268	1.179	0.678	118.64	11.32	3.87
^{58}Ni+^{124}Sn	AW	83.338	1.180	0.687	160.70	11.69	3.68
^{64}Ni+^{124}Sn	AW	82.496	1.180	0.690	158.52	11.86	3.52

C. Systematics of the fusion suppression factor

A systematic study of the suppression factor for CF (F_{CF}) as a function of the charge product of the projectile and target ($Z_P Z_T$) for different reactions involving weakly bound projectiles has been reported by Gasques *et al.* [12]. They showed that (i) for a particular projectile, the suppression factor is more or less independent of the product $Z_P Z_T$, and (ii) suppression increases with deceasing breakup threshold of the projectile. However, the reactions involving ^{9}Be did not follow this systematic trend. So it would be interesting to see if there is anything special about ^{9}Be nuclei. To investigate this systematics further with other reactions involving ^{9}Be as a projectile, we included the results for the present ^{9}Be+^{124}Sn reaction and, also, the data on ^{9}Be+^{209}Bi from Ref. [7]. The results for these systems, along with other reactions involving weakly bound projectiles reported earlier [12], are shown in Fig. 6. It was observed that the suppression factor F_{CF} for reactions involving ^{9}Be as a projectile, with ^{124}Sn, ^{208}Pb, and ^{209}Bi targets, are similar and agree with the systematic

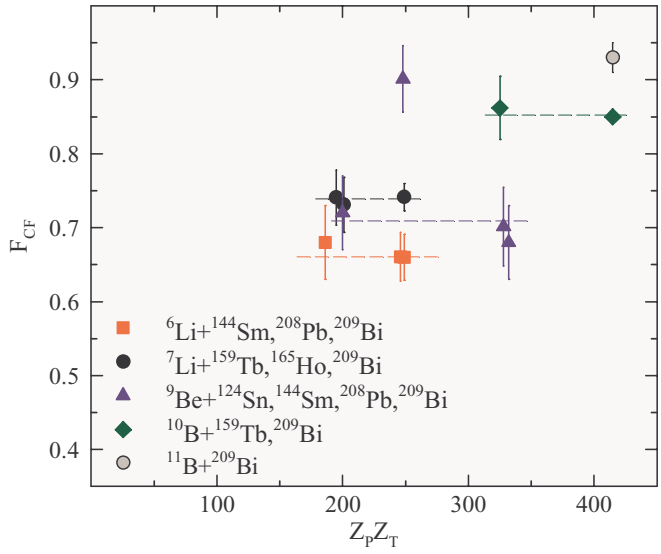

FIG. 6. (Color online) The complete fusion suppression factor F_{CF} at above-barrier energies as a function of the charge product of projectile and target (adopted from Ref. [12]). The reactions considered are ^{6}Li incident on ^{144}Sm [19], ^{208}Pb [25], and ^{209}Bi [6] targets; ^{7}Li incident on ^{159}Tb [5], ^{165}Ho [3], and ^{209}Bi [6] targets; ^{9}Be incident on ^{144}Sm [8], ^{208}Pb [6], and ^{209}Bi [7] targets and the present work on a ^{124}Sn target; ^{10}B incident on ^{159}Tb [5] and ^{209}Bi [12] targets; and ^{11}B incident on a ^{209}Bi [12] target. Lines are to guide the eye.

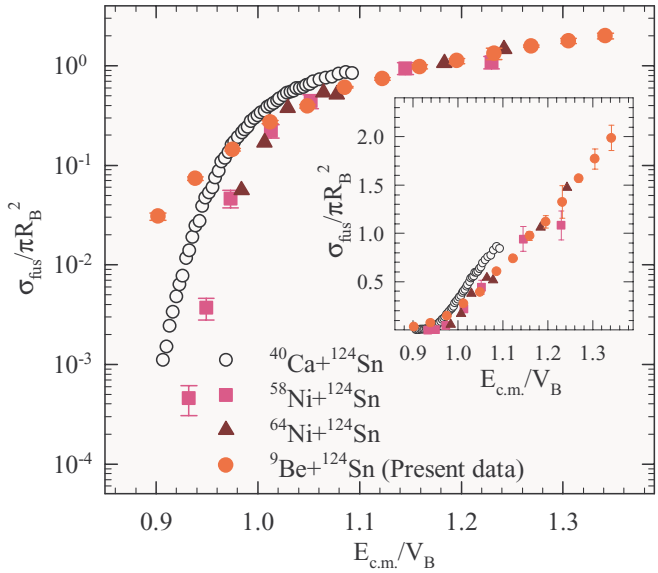

FIG. 7. (Color online) Reduced fusion cross sections for ^{40}Ca+^{124}Sn [26], ^{58}Ni+^{124}Sn [27,28], and ^{64}Ni+^{124}Sn [29] and for the present data (CF cross sections) on ^{9}Be+^{124}Sn. Inset: the same figure on a linear scale.

trend observed by Gasques *et al.* However, the behavior of the ^{9}Be+^{144}Sm reaction (a nearby system) is surprisingly different and difficult to understand.

D. Reduced fusion cross sections for different reactions involving a ^{124}Sn target

We compared the reduced fusion cross sections $\sigma_{fus}/\pi R_B^2$ vs. $E_{c.m.}/V_B$ for different projectiles on a ^{124}Sn target. The fusion excitation functions of ^{40}Ca+^{124}Sn [26], ^{58}Ni+^{124}Sn [27,28], and ^{64}Ni+^{124}Sn [29] were utilized for this purpose. Note that the fusion cross sections of ^{9}Be+^{124}Sn are CF cross sections, while the others are for total fusion (i.e., the sum of CF and ICF) cross sections. The fusion barrier height (V_B) and radius (R_B) were deduced from the AW potentials. The potentials used and the corresponding values of V_B and R_B are listed in Table II. The corresponding reduced fusion cross sections for different reactions involving ^{124}Sn as the target are shown in Fig. 7. It can be concluded from this figure that the reduced fusion cross sections for ^{9}Be projectiles are enhanced at energies below the barrier, possibly owing to the extended structure of its weakly bound cluster. At above-barrier energies, owing to the high breakup probability, one would a priori expect the CF for ^{9}Be to be suppressed compared to the total fusion for tightly bound nuclei. Interestingly, it is observed (as shown in the inset in Fig. 7) that CF for ^{9}Be is suppressed compared to total fusion for ^{40}Ca, but similar to total fusion for ^{58,64}Ni. In a study of the ^{58}Ni+^{124}Sn reaction [30], it was found that the fusion cross sections at energies above the barrier are smaller compared to those predicted by the semiclassical calculations. It was also concluded that the presence of a large cross section for deep inelastic scattering at these energies could inhibit the formation of a compound nucleus, an effect that has been interpreted in terms of the extra-push model of Swiatecki [31]. However, it could also be possible to have a large cross section of multinucleon exchange from the projectile (^{58,64}Ni) to the target (^{124}Sn), leading to transfer/ICF and, thereby, reducing the CF probability. As ^{40}Ca is a doubly shell-closed nucleus, it has a higher probability of compound nucleus formation compared to ^{58,64}Ni. Interestingly, the extent of suppression for ^{58,64}Ni-induced systems is of an order similar to that of ^{9}Be, although they may be caused by different mechanisms.

Enhancement of fusion cross sections involving a weakly bound projectile like ^{9}Be at sub-barrier energies has not been well described in the available literature so far. However, there exists a difference in the behavior of fusion data involving weakly bound projectiles between sub- and above-barrier regimes. More data emphasizing this feature are necessary to verify the foregoing observation.

IV. SUMMARY

The fusion excitation function for the ^{9}Be+^{124}Sn reaction in the energy range $0.90 < V_b < 1.34$ has been measured using an online γ-ray technique. At above-barrier energies, the measured CF cross sections were found to be suppressed by a factor of 28(±5)% compared to the CC calculations. Surprisingly, the suppression factor is very different from the value for the nearby system ^{9}Be+^{144}Sm. However, the systematic dependence of the CF suppression factor for ^{9}Be-induced fusion reactions, as a function of the charge product of the projectile and target (Z_PZ_T), is consistent with the results involving other weakly bound projectiles. In the study of projectile dependence, the comparison of the reduced fusion cross section for several reactions involving a ^{124}Sn target shows significant enhancement in fusion at below-barrier

energies for ^{9}Be projectiles. More systematic data on fusion cross sections for different projectiles on the same target are necessary to verify the aforementioned enhancement behavior and understand the reaction mechanism.

A separate off-line γ-ray measurement of the ^{9}Be+^{124}Sn reaction over a similar energy range is being planned to extract the cross sections for the remaining ICF channel (^{127}Te) and $1n$ transfer channel (^{125}Sn), both of which decay by β radiation, having measurable half-lives. This will determine the loss of flux, causing the suppression [$F_{CF} = 0.72(5)$] of CF, that appears in the preceding two unobserved channels.

ACKNOWLEDGMENTS

The authors would like to thank the Pelletron crew for their smooth operation of the accelerator during the experiment and P. Das for supplying the ^{124}Sn target. We would also like to thank A. Mukherjee for useful discussions.

[1] L. F. Canto, P. R. S. Gomes, R. Donangelo, and M. S. Hussein, Phys. Rep. **424**, 1 (2006), and references therein.
[2] G. D. Dracoulis, A. P. Byrne, T. Kibedi, T. R. McGoram, and S. M. Mullins, J. Phys. G **23**, 1191 (1997); A. Jungclaus *et al.*, Phys. Rev. C **66**, 014312 (2002); S. Sihotra *et al.*, *ibid.* **78**, 034313 (2008).
[3] Vandana Tripathi, A. Navin, K. Mahata, K. Ramachandran, A. Chatterjee, and S. Kailas, Phys. Rev. Lett. **88**, 172701 (2002).
[4] J. Takahashi, M. Munhoz, E. M. Szanto, N. Carlin, N. Added, A. A. P. Suaide, M. M. de Moura, R. Liguori Neto, A. Szanto de Toledo, and L. F. Canto, Phys. Rev. Lett. **78**, 30 (1997).
[5] A. Mukherjee *et al.*, Phys. Lett. B **636**, 91 (2006).
[6] M. Dasgupta *et al.*, Phys. Rev. C **70**, 024606 (2004).
[7] M. Dasgupta, D. J. Hinde, S. L. Sheehy, and B. Bouriquet, Phys. Rev. C **81**, 024608 (2010).
[8] P. R. S. Gomes *et al.*, Phys. Rev. C **73**, 064606 (2006).
[9] G. V. Marti *et al.*, Phys. Rev. C **71**, 027602 (2005).
[10] S. B. Moraes, P. R. S. Gomes, J. Lubian, J. J. S. Alves, R. M. Anjos, M. M. Sant'Anna, I. Padrón, C. Muri, R. Liguori Neto, and N. Added, Phys. Rev. C **61**, 064608 (2000); R. M. Anjos *et al.*, Phys. Lett. B **534**, 45 (2002); P. R. S. Gomes *et al.*, *ibid.* **601**, 20 (2004); Phys. Rev. C **71**, 034608 (2005).
[11] D. J. Hinde, M. Dasgupta, B. R. Fulton, C. R. Morton, R. J. Woolliscroft, A. C. Berriman, and K. Hagino, Phys. Rev. Lett. **89**, 272701 (2002).
[12] L. R. Gasques, D. J. Hinde, M. Dasgupta, A. Mukherjee, and R. G. Thomas, Phys. Rev. C **79**, 034605 (2009); M. Dasgupta, L. R. Gasques, D. H. Luong, R. du Rietz, R. Rafiei, D. J. Hinde, C. J. Lin, M. Evers, and A. Diaz-Torres, Nucl. Phys. A **834**, 147c (2010).
[13] T. Lönnroth, J. Hattula, H. Helppi, S. Juutinen, K. Honkanen, and A. Kerek, Nucl. Phys. A **431**, 256 (1984).
[14] J. N. Orce *et al.*, Phys. Rev. C **74**, 034318 (2006).
[15] C. T. Zhang *et al.*, Nucl. Phys. A **628**, 386 (1998).
[16] Z. Zhao, J. Yan, A. Gelberg, R. Reinhardt, W. Lieberz, A. Dewald, R. Wirowski, K. O. Zell, and P. von Brentano, Z. Phys. A **331**, 113 (1988); H. Helppi, J. Hattula, A. Luukko, M. Jaaskelainen, and F. Donau, Nucl. Phys. A **357**, 333 (1981).
[17] A. Gavron, Phys. Rev. C **21**, 230 (1980).
[18] K. Hagino, N. Rowley, and A. T. Kruppa, Comput. Phys. Commun. **123**, 143 (1999).
[19] P. K. Rath *et al.*, Phys. Rev. C **79**, 051601(R) (2009).
[20] K. Hagino (private communication).
[21] R. A. Broglia and A. Winther, *Heavy Ion Reactions, Lecture Notes Vol. I* (Addison-Wesley, Redwood City, CA, 1991), p. 114.
[22] H. J. Votava, T. B. Clegg, E. J. Ludwig, and W. J. Thompson, Nucl. Phys. A **204**, 529 (1973).
[23] H. Nguyen Ngoc, M. Hors, and J. Perez-y-Jorba, Nucl. Phys. **42**, 62 (1963).
[24] Shrabani Sinha, M. R. Pahlavani, R. Varma, R. K. Choudhury, B. K. Nayak, and A. Saxena, Phys. Rev. C **64**, 024607 (2001).
[25] Y. W. Wu, Z. H. Liu, C. J. Lin, H. Q. Zhang, M. Ruan, F. Yang, Z. C. Li, M. Trotta, and K. Hagino, Phys. Rev. C **68**, 044605 (2003).
[26] F. Scarlassara, S. Beghini, G. Montagnoli, G. F. Segato, D. Ackermann, L. Corradi, C. J. Lin, A. M. Stefanini, and L. F. Zheng, Nucl. Phys. A **672**, 99 (2000).
[27] F. L. H. Wolfs, Phys. Rev. C **36**, 1379 (1987).
[28] W. S. Freeman, H. Ernst, D. F. Geesaman, W. Henning, T. J. Humanic, W. Kuhn, G. Rosner, J. P. Schiffer, B. Zeidman, and F. W. Prosser, Phys. Rev. Lett. **50**, 1563 (1983).
[29] K. T. Lesko, W. Henning, K. E. Rehm, G. Rosner, J. P. Schiffer, G. S. F. Stephans, B. Zeidman, and W. S. Freeman, Phys. Rev. Lett. **55**, 803 (1985).
[30] G. Pollarolo, Nucl. Phys. A **787**, 206c (2007).
[31] W. J. Swiatecki, Phys. Scr. **24**, 113 (1981); Nucl. Phys. A **376**, 275 (1982).